NUMERICAL HEAT TRANSFER, PART B: FUNDAMENTALS
https://doi.org/10.1080/10407790.2023.2282165

Taylor & Francis
Taylor & Francis Group

An analysis of heat and mass transfer of ternary nanofluid flow over a Riga plate: Newtonian heating

U.S. Mahabaleshwar[a], K.M. Nihaal[a], L.M. Pérez[b], and H. F. Oztop[c,d,e]

[a]Department of Studies in Mathematics, Shivagangotri, Davangere University, India; [b]Departmento de Física, FACI, Universidad de Tarapacá, Arica, Chile; [c]Department of Mechanical and Nuclear Engineering, College of Engineering, University of Sharjah, United Arab Emirates; [d]Department of Mechanical Engineering, Firat University, Elazig, Turkey; [e]Department of Medical Research, China Med. University Hospital, China Med. University, Taichung, Taiwan

ABSTRACT

Ternary nanofluids have been show cased to substantially enhance the thermal conductivity and heat transfer attributes of base fluids when compared to ordinary fluids, nanofluids, and hybrid nanofluids. As expected, they are beneficial in thermal management and cooling, and other applications that require effective heat transference. The present analysis deals with the ternary nanofluid flow with heat transmission across Riga plate considering Newtonian heating effect. Fe_2O_4, ZnO, and $CoFe_2O_4$ are in a base fluid H_2O creating a unique combination of $Fe_2O_4 - ZnO - CoFe_2O_4 - H_2O$ that offers various physical and chemical properties. Using appropriate similarity variables, the controlling PDEs are deformed to ODEs, that are analyzed *via* shooting method and byp4c algorithm. The consequences of several parameters are discussed Graphical on temperature, concentration, and velocity profiles are shown. The outcome of the present analysis shows that in the presence of a Newtonian heating effect, the temperature profile shows better thermal performance than in the absence of the Newtonian heating effect. Additionally, the nature of certain significant engineering coefficients for specific parameters is studied in this article. It is seen that the heat source elevates the rate of heat transfer between a solid surface and fluid flow, whereas opposite trend is observed when the heat sink is considered. Also, the rate of mass transfer is achieved by rising values of the chemical reaction parameter.

ARTICLE HISTORY
Received 20 July 2023
Revised 2 October 2023
Accepted 21 October 2023

KEYWORDS
Chemical reaction; inclined magnetic field; nonlinear heat/source sink; Newtonian heating; stagnation point; ternary nanofluid

1. Introduction

Ultra-high thermal performance is one of the most vital needs of many automobile industries. Generally, thermal system radiators, engine oils, coolants, and other high-temperature heat transfer fluids found in typical trucks have inherently poor heat transfer properties. This could be benefited by employing nanofluids resulting from nanoparticles addition (typically 1–100nm) that offer high thermal conductivity compared to conventional fluids [1]. Choi and Eastman [2] were the first to explore nanofluid thermal properties, and they explained that these fluids show superior heat transfer to those of host fluids. In order to enhance fluid thermal conductivity beyond that of conventional mono and hybrid-material type nanofluid, Manjunath et al. [3] did the initial survey to examine the thermophysical properties of the ternary nanofluid model. Due to its high thermal efficiency, it has many industrial applications such as heat exchangers in power plants,

CONTACT H. F. Oztop hfoztop1@gmail.com Department of Mechanical Engineering, Firat University, Elazig, Turkey; K.M. Nihaal, nihaal.kmdvg@gmail.com Department of Studies in Mathematics, Shivagangotri, Davangere University, India.

Nomenclature

U_∞	ambient fluid velocity (ms^{-2})
T_∞	ambient temperature (K)
(x, y)	Cartesian coordinates (m)
$a,\ d$	constants
$U_w(x)$	constant velocity (ms^{-2})
C_w	concentration at wall $(mol\ m^{-3})$
C_∞	concentration at far field $(mol\ m^{-3})$
j_0	current density (Am^{-2})
A_1, A_2, A_3, A_4	constants
K_c	chemical reaction parameter (s^{-1})
D	diffusivity $(\ m^2s^{-1})$
Ha	Hartman number
h_s	heat transfer coefficient (W/m^2K)
M_0	magnetization of permanent magnets
M	magnetic parameter (T)
B_0	magnetic field (A/m^2)
q_m	mass heat flux $(mol\ s^{-1}\ m^{-2})$
q'''	nonlinear heat source/sink parameter $(kgm^{-1}s^{-3})$
$A^*,\ B^*$	parameters of the space-dependent and temperature-dependent internal heat generation/absorption
Pr	Prandtl number
Re	Reynolds number
Sc	Schmidt number
(u, v)	velocity components (ms^{-2})
T_w	wall temperature (K)
Cp	specific heat $(J\ kg^{-1}K^{-1})$
k	thermal conductivity $(kgms^{-3}K^{-1})$
q_w	wall heat flux (kgs^{-3})
μ	dynamic viscosity $(kgm^{-1}s^{-1})$
ρ	density (kgm^{-3})
σ	electrical conductivity $(\Omega^{-1}m^{-1})$
τ	inclination angle
ν	kinematic viscosity (m^2s^{-1})
β	width of magnets and electrodes (m)
α	thermal diffusivity (m^2s^{-1})
φ	solid volume fraction
γ	Newtonian heating parameter
τ_w	shear stress at the wall $(kgm^{-1}s^{-2})$

Subscripts

nf	nanofluid
hnf	hybrid nanofluid
tnf	ternary nanofluid

Abbreviations

BLF	boundary layer flow
CWT	common wall temperature
MHD	magnetohydrodynamics

manufacturing processes, cancer treatments, and automotive parts [4]. Yang et al. [5] applied the Artificial Neural Network model to examine the thermal conductivity of ternary nanofluids made of carbon-based materials, titania, and zinc oxide. Recently, using a ternary nanofluid, Kopp et al. [6] studied Brownian diffusion and thermophoretic effects with MHD.

The fluid flow with the magneto-hydrodynamic (MHD) effect having many applications such as the design of liquid metal cooling systems, MHD power production, accelerators, pumps, and magnetic drug targeting [7–13] some researchers conducted study using MHD are . Because of such applications, numerous researchers have researched peristaltic motion problems under the magnetic influence. Nadeem and Akram [14] inspected the impact of inclined MHD on peristaltic flow in an inclined symmetric/asymmetric Williamson Fluid channel. In his research, Aslani et al. [15] considered micropolar flow through the porous medium on a stretching/shrinking surface for the study of the joint effect of inclined MHD radiation and mass transpiration effect. Employing inclined MHD, Mahabaleshwar et al. [16] brought up an analytical method to investigate key role of carbon nanotubes under the influence of Newtonian heating and radiation effect over-stretching stretching and shrinking sheets. Recently, a notable work on MHD was done by, Selimefendigil and Öztop [17] and Manna et al. [18].

The fluid flow at the stagnation point becomes a more interesting area among researchers due to its wide applications in engineering. A stagnation point in a flow stream is a place in which the velocity of a fluid is nil with a stronger pressure gradient. The concept of stagnation point flow may be found practically everywhere in technological applications such as axial fan designs, nuclear reactor cooling, and also in aerodynamics applications. The pioneering work on this concept was done by Hiemenz [19], he proposed a numerical study on steady viscous stagnation point flow. Subsequently, an analytical study on axisymmetric stagnation point flow was put forward by Homann [20]. Afterward, Howarth [21] did an extension of this study for better results.

Stagnation point flow in the presence of MHD in an extended surface was examined by Ishak et al. [22]. Anusha et al. [23] examined unsteady non-non-Newtonian Casson fluid flow on a flat plate with combine effect of MHD and radiation.

Heat absorption/generation is a huge phenomenon nowadays in many industrial applications because it has a significant impact on flow stability. Heat generation/absorption is a temperature-dependent phenomenon that is extremely important in the thermal convectional process where there is substantial temperature variation along the plate and the far-field fluid. It has other several applications such as in semiconductors, electronic chips, and nuclear power reactors. Many researchers are showing their interest to explore the effects of heat absorption/generation on various factors such as Ashwinkumar [24], Poojari et al. [25], Sandeep et al. [26], Nanda et al. [27], Sandeep et al. [28]. Abel et al. [29] examine the physical properties of viscoelastic fluids flowing across stretched surface with MHD being present with an influence of a nonuniform heat generation. In order to account for the impacts of internal heat generation/absorption and frictional heating, Vajravelu and Hadjinicolaou [30] examined the heat transmission properties on a constantly linear stretched sheet with impact of a viscous fluid. *via* highly conducting micropolar fluids, Pal and Mandal [31] conducted a numerical study to look into the consequences of nonuniform heat generation/absorption and radiation across a stretched sheet with MHD.

The development of methods for predicting thermal circulation between fluid bodies in the occurrence of chemical reactions has sparked the interest of many researchers in the current state because of its vital impact in managing mass and heat transfer in many chemical industries. Motulevich [32] was the first to investigate the impact of chemical reactions on heat transport phenomena. Mahabaleshwar et al. [33] scrutinized the impact caused by radiation, chemical reaction with a heat sink/source over a thermosolutal Marangoni flow on a porous media. In a perpendicular channel with a couple stress fluid considering heat source/sink employing first order reactions, Mallikarjun et al. [34] developed computational methods for the flow of mixed convection. Sandeep et al. [35] explored the dynamics of Casson liquid flow over a curved surface using chemical reaction.

There are numerous industrial applications for Newtonian heating in solar radiation, oil industries, and heat exchangers. Newtonian heating boosts fluid flow by acting as a foster agent. Merkin [36] pioneered the study of Newtonian heating in 1994. In his work, he investigated natural convection along the boundary layer movement (BL) produced by NH (Newtonian heating). Various researchers have recently investigated NH effects due to their real-world applications [37,38]. Due to its unique electromagnetic surface, the Riga plate can generate MHD behavior in fluid flow. In 1961, pioneering research was done by Gailitis and Lielausis [39]. Later, his work was carried out by many researchers. Eugen Magyari and Asterios Pantokratoras [40] investigated opposing and assisting mixed convective flow on the Riga plate. Recently, Using Particle Swarm Optimization (PSO), Upreti et al. [41] analyzed the nature of heat and diffusion transmission in a Casson nano-based liquid containing microbes on Riga plate. Khashi'i.e. et al. [42] studied an unstable isolated stagnation point flow under EMHD conditions and heat generation on a Riga plate.

The aforementioned study indicates that TNF has important scientific applications in a variety of fields (engineering and industrial) due to its much higher heat transfer rate than conventional fluids. This current research is extension of Ahmed et al. [43] comprising of ternary nanofluids with addition of magnetic field, nonlinear heat source/sink, and chemical reaction. The three nanoparticles Fe_2O_4, ZnO, and $CoFe_2O_4$ possess numerous industrial and scientific applications due to its magnetic properties. Hence for better heat transfer these above-mentioned nanoparticles are considered.

2. Mathematical modeling

The following assumptions are considered while making a modeling of the study. The flow of the liquid is steady, two-dimensional, and incompressible in nature. Further, the geometry Riga surface is normal to the y-axis, and u, v represents velocity units of the coordinate axis x, y.

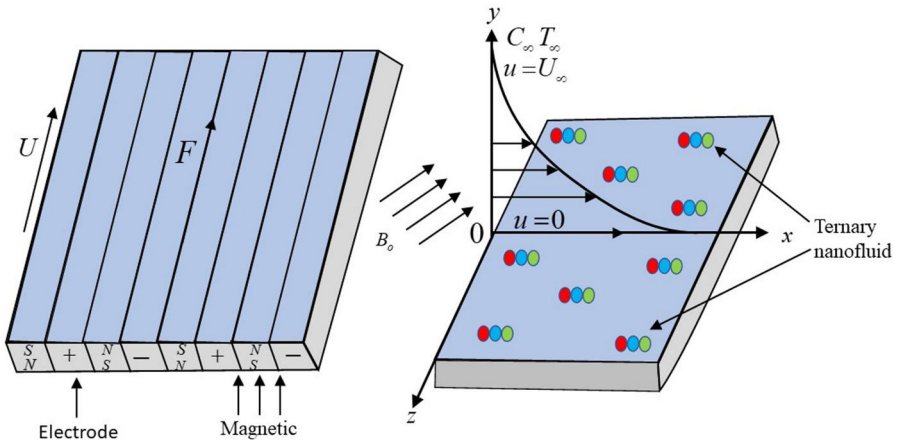

Figure 1. Schematic diagram of the flow problem.

Magnetic effects, nonuniform heat absorption/generation effects, Newtonian heating and chemical reaction effects are considered. Further, it is expected that Riga approaches free stream velocity $U_w(x) = ax$ with x axis and is warmed on a custom basis by an imposed temperature T_w. T_w and T_∞ denotes wall and ambient fluid temperature, C_w and C_∞ are concentration at wall (i.e., $y = 0$) and beyond boundary layer (i.e., $y \to \infty$) at the Riga plate respectively (see Figure 1) and $u = 0$ and $v = 0$ denotes the boundary conditions for velocity profile at $y = 0$ and as $y \to \infty$ the horizontal velocity reach to U_∞, i.e. $u \to U_\infty$. The governing equations can be expressed using the Oberbeck-Boussinesq model as follows [43–45].

$$\frac{\partial v}{\partial y} + \frac{\partial u}{\partial x} = 0, \tag{1}$$

$$v\frac{\partial u}{\partial y} + u\frac{\partial u}{\partial x} = \nu_{tnf}\frac{\partial^2 u}{\partial y^2} + a^2 x + \frac{\pi j_o M_o}{8\rho_{tnf}} e^{-\frac{\pi}{\beta}y} - \frac{\sigma_{tnf} B_o^2 \sin^2 \tau}{\rho_{tnf}} u, \tag{2}$$

$$v\frac{\partial T}{\partial y} + u\frac{\partial T}{\partial x} = \frac{q''\prime}{(\rho C_p)_{tnf}} + \alpha_{tnf}\frac{\partial^2 T}{\partial y^2}, \tag{3}$$

$$u\frac{\partial C}{\partial x} + v\frac{\partial C}{\partial y} = D_{tnf}\frac{\partial^2 C}{\partial y^2} - K_c^2(C - C_\infty). \tag{4}$$

The above equations are subjected to following bcs,

$$\left.\begin{array}{llllll} u = 0, & \dfrac{\partial T}{h_s \partial y} = -T(NH), & v = 0, & C = C_w & \text{at} & y = 0 \\ u \to U_\infty, & T \to T_\infty \ (CWT), & C \to C_\infty & & \text{at} & y \to \infty \end{array}\right\} \tag{5}$$

Here, q''' is the nonuniform heat source sink given by [45],

$$q''' = \frac{k_f U_w(x)}{x\nu_f}\left[A * (T_w - T_\infty)f' - (T_\infty - T)B*\right]. \tag{6}$$

In the above Eq. (6), the term $B*$ is temperature and $A*$ is space dependent internal heat absorption/generation.

Thermophysical properties with expressions of ternary nanoparticles are given below [33],

$$\mu_{tnf} = \frac{\mu_f}{(1-(\varphi_1+\varphi_2+\varphi_3))^{2.5}},\quad \rho_{tnf} = (1-\varphi_1)\big((1-\varphi_2)\big[(1-\varphi_3)\rho_f + \rho_{S3}\varphi_3\big] + \rho_{S2}\varphi_2\big) + \rho_{S1}\varphi_1,$$

$$(\rho C_p)_{tnf} = \left(\frac{(\rho C_p)_{S1}\varphi_1}{(\rho C_p)_f} + (1-\varphi_1)\left[(1-\varphi_2)\left((1-\varphi_3) + \frac{(\rho C_p)_{S3}\varphi_3}{(\rho C_p)_f}\right) + \frac{(\rho C_p)_{S2}\varphi_2}{(\rho C_p)_f}\right]\right)(\rho C_p)_f,$$

$$\sigma_{tnf} = \left(\frac{\sigma_{S1}(1+2\varphi_1) + \sigma_{hnf}(1-2\varphi_1)}{\sigma_{S1}(1-\varphi_1) + \sigma_{hnf}(1+\varphi_1)}\right)\sigma_{hnf},\quad \sigma_{hnf} = \left(\frac{\sigma_{S2}(1+2\varphi_2) + \sigma_{nf}(1-2\varphi_2)}{\sigma_{S2}(1-\varphi_2) + \sigma_{nf}(1+\varphi_2)}\right)\sigma_{nf},$$

$$\sigma_{nf} = \left(\frac{\sigma_{S3}(1+2\varphi_3) + \sigma_{nf}(1-2\varphi_3)}{\sigma_{S3}(1-\varphi_3) + \sigma_{nf}(1+\varphi_3)}\right)\sigma_f.$$

$$k_{tnf} = \left(\frac{k_{S1} + 2k_{hnf} - 2\varphi_1(k_{hnf} - k_{S1})}{k_{S1} + 2k_{hnf} + \varphi_1(k_{hnf} - k_{S1})}\right)k_{hnf},\quad k_{hnf} = \left(\frac{k_{S2} + 2k_{nf} - 2\varphi_2(k_{nf} - k_{S2})}{k_{S2} + 2k_{nf} + \varphi_2(k_{nf} - k_{S2})}\right)k_{nf},$$

$$k_{nf} = k_f\left(\frac{k_{S3} + 2k_f - (k_f - k_{S3})2\varphi_3}{k_{S3} + 2k_f + (\varphi_3 k_f - \varphi_3 k_{S3})}\right),\quad D_{tnf} = (1-(\varphi_1+\varphi_2+\varphi_3))^{2.5} D_f$$

where C_p-specific heat capacity, electrical conductivity and thermal conductivity are represented by σ and k, respectively, μ and ρ denotes dynamic viscosity and density. And φ_1, φ_2, φ_3 are volume fractions of nanoparticles mentioned in following Table 1.

2.1. Similarity analysis

$$\eta = \sqrt{\frac{a}{\nu_f}}y,\quad u = ax\, f'(\eta),\quad \frac{\nu}{f(\eta)} = -\sqrt{a\ \nu_f} \tag{7}$$

$$(CWT)\theta(\eta) = \frac{T - T_\infty}{T_w - T_\infty},\quad (NH) : \theta(\eta)T_\infty = T - T_\infty,\quad C = C_\infty + (C_w - C_\infty)\chi(\eta) \tag{8}$$

Now by introducing the above similarity variables, governing Eqs. (1)–(4) and Bcs. (5–6) are transmuted into non similar ODEs.

$$f''' + \mathrm{A_1A_2}\left(ff'' - f'2 + \frac{Ha}{A_3}\ e^{-d\eta} - \frac{\sigma_{tnf}}{\sigma_t}\frac{M}{\mathrm{A_3}}f'\ \sin(\tau) + 1\right) = 0, \tag{9}$$

$$\theta'' + \frac{1}{\mathrm{A_4}}\left(B^*\theta + A^*f'\right) + \mathrm{Pr}\left(\frac{\mathrm{A_3}}{\mathrm{A_4}}\right)\theta' f = 0, \tag{10}$$

$$\chi'' + Sc(f\chi') - Sc\ Kc\ \chi = 0. \tag{11}$$

With corresponding Bcs:

Table 1. Thermophysical characteristics [46].

	H_2O	Fe_2O_4	ZnO	$CoFe_2O_4$
Density	997.1	5180	5606	4907
Specific heat capacity	4179	670	544	700
Thermal heat conductivity	0.613	9.7	19	1.3×10^{-5}
Electric conductivity	0.05	25000	0.01	1.1×10^{7}

$$\begin{aligned}&\eta = 0: \quad \chi(0) = 1, \quad f(0) = 0, \quad f'(0) = 0,\\ &\theta(0) = 1(CWT - Case), \ \theta'(0) = -\gamma(\theta(0)+1)(NH - Case)\}\\ &\eta \to \infty : f'(\infty) \to 1, \quad \theta(\infty) \to 0, \quad \chi(\infty) \to 0\end{aligned} \tag{12}$$

Here, $\gamma = h_s\sqrt{\frac{\nu_f}{a}}$ is conjugate parameter for Newtonian heating,

$$\mathrm{A}_1 = (1-\varphi_1-\varphi_2-\varphi_3)^{2.5}, \ \mathrm{A}_2 = (1-\varphi_1)^{2.5}\left((1-\varphi_2)\left[(1-\varphi_3)+\frac{\rho_{S3}}{\rho_f}\varphi_3\right]+\frac{\rho_{S2}}{\rho_f}\varphi_2\right)+\frac{\rho_{S1}}{\rho_f}\varphi_1,$$

$$\mathrm{A}_3 = \left(\frac{(\rho C_p)_{S1}\varphi_1}{(\rho C_p)_f}+(1-\varphi_1)\left[(1-\varphi_2)\left((1-\varphi_3)+\frac{(\rho C_p)_{S3}\varphi_3}{(\rho C_p)_f}\right)+\frac{(\rho C_p)_{S2}\varphi_2}{(\rho C_p)_f}\right]\right), \ \mathrm{A}_4 = \frac{k_{tnf}}{k_f},$$

$D_{tnf} = A_1 D_f$, $d = \frac{\pi}{\beta}\sqrt{\frac{\nu_f}{a}}$ is dimensionless parameter, $Ha = \frac{\pi j_o Mo}{8\rho_f a^2 x}$ is the modified Hartmann number, $M = \frac{\sigma_f B_o^2}{\rho_f}$ represents Magnetic parameter, $\mathrm{Pr} = \frac{\nu_f(\rho C_p)_f}{k_f}$ is known as Prandtl number, $Sc = \frac{\nu_f}{D}$ is Schmidt number, $Kc = \frac{K^2}{a}$ is referred as chemical reaction constraint.

The significant engineering coefficients like Sherwood number, Skin-friction, and local Nusselt number is given, along with their simplified forms [47].

$$sh_x = \frac{xq_m}{D_f(C_w - C_\infty)} \ \text{ where, } \ q_m = -D_{tnf}\left.\frac{\partial C}{\partial y}\right|_{y=0} \tag{13}$$

$$Cf_x = \frac{\tau_w(x)}{\rho_f \ U_\infty^2} \ \text{ where, } \ \tau_w(x) = \mu_{tnf}\left.\frac{\partial u}{\partial y}\right|_{y=0} \tag{14}$$

$$Nu_x = \frac{xq_w}{k_f(T_w - T_\infty)} \ \text{ where, } \ q_w = -k_{tnf}\left.\frac{\partial T}{\partial y}\right|_{y=0} \tag{15}$$

$$\mathrm{Re}^{1/2}Cf_x = \frac{f''(0)}{\mathrm{A}_1}, \ \mathrm{Re}^{-1/2}Nu_x = -\mathrm{A}_4 \ \theta'(0), \ sh_x = -A_1\chi'(0)\mathrm{Re}^{1/2} \tag{16}$$

where $\mathrm{Re} = \frac{U_\infty(x)x}{\nu_f}$.

2.2. Numerical procedure

Using the computational tool byp4c with shooting technique, the set of reduced Eqs. (9)–(10) and reduced BCs in (12) are solved. Due to the high order of converted equations and two-point boundary nature of the equations that were obtained. They are converted into first order system to obtain solutions by replacing as follows:

On Deducing $\left\langle \begin{matrix} f, f', f'', \\ \theta, \theta', \\ \chi, \chi' \end{matrix} \right\rangle = \left\langle \begin{matrix} y_1, y_2, y_3, \\ y_4, y_5, \\ y_6, y_7 \end{matrix} \right\rangle$ the equations become,

$$f''' = -\mathrm{A}_1\mathrm{A}_2\left[y_1y_3 - y_2^2 + Ha \ e^{-dn} - M\sin(\tau)y_2 + 1\right] \tag{17}$$

$$\theta'' = -\left[\frac{1}{\mathrm{A}_4}(A * y_2 + B * y_5) + \left(\frac{\mathrm{A}_3}{\mathrm{A}_4}\right)\mathrm{Pr}y_1y_5\right] \tag{18}$$

$$\chi'' = Sc(-y_1y_7 + \ Kcy_6) \tag{19}$$

And Bcs. becomes,

Table 2. Computational results of the skin-friction coefficient $f''(0)$ for different values *Ha* and *d* with $\mathrm{Pr} = 6.2$, $d = 0.5$, $Sc = 0.5$, $Bi = 50$.

		$f''(0)$[43]		$f''(0)$	
Ha	*d*	Shooting	bcp4c	Shooting	bcp4c
0	0.5	1.4294038	1.4294037	1.4293998	1.4294020
0.5	0.5	1.7243537	1.7243587	1.7243619	1.7243619
1.0	0.5	2.0099196	2.0099297	2.0099090	2.0099196
1.5	0.5	2.2874751	2.2874603	2.2869977	2.2869997
1.0	0	1.5394682	1.5394732	1.5394651	1.5394698
1.0	1	1.9023442	1.9023488	1.9023450	1.9023481
1.0	2	2.2416224	2.2416273	2.2416219	2.2416278
1.0	3	2.5631502	2.5631452	2.5631499	2.5631455

Table 3. Computational results of local Nusselt number $-\theta'(0)$ at various values of *Ha*, *d*, and γ with other parameters $\mathrm{Pr} = 6.2$, $Sc = 0.5$, $Kc = 0.5$.

			$-\theta'(0)$[43]		$-\theta'(0)$	
Ha	*d*	γ	Shooting	bvp4c	Shooting	bvp4c
0	0.5	5	0.52262732	0.52262707	0.52262700	0.52262701
0.5	0.5	5	0.55588512	0.55592229	0.55588519	0.55592225
1.0	0.5	5	0.58383262	0.58389767	0.58383265	0.58389763
0.5	0.1	5	0.56029900	0.56030037	0.56029889	0.56030034
0.5	0.2	5	0.55592167	0.55592274	0.55592159	0.55592277
0.5	0.3	5	0.55232480	0.55232517	0.55232476	0.55232511
0.5	0.5	0	0.0	0.0	0.0	0.0
0.5	0.5	0.5	0.27715283	0.27715312	0.27715284	0.27715311
0.5	0.5	1.0	0.38397307	0.38397360	0.38397310	0.38397363

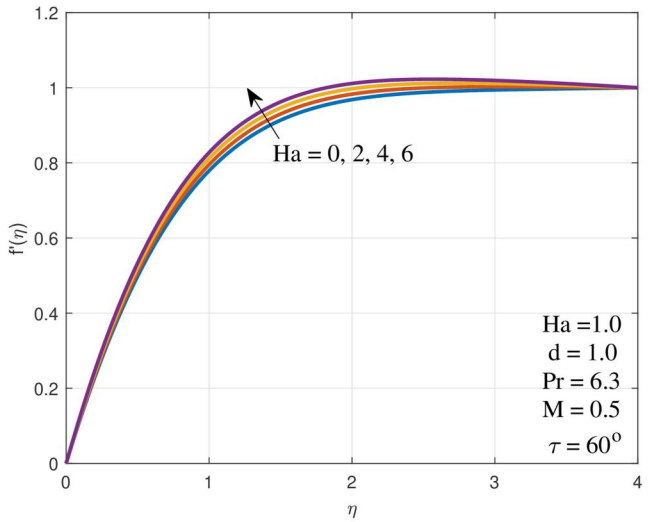

Figure 2. Plot of $f\prime(\eta)$ for different values of *Ha*.

$$\begin{bmatrix} f(0) = 0, \\ f'(0) = 0, \\ f'(\infty) \to 1, \\ \theta(0) = 1, \\ \theta'(0) = -\gamma(1 + \theta(0)), \\ \theta(\infty) \to 0, \\ \chi(0) = 1, \\ \chi(\infty) \to 0 \end{bmatrix} = \begin{bmatrix} \mathrm{ya}_1 \\ \mathrm{ya}_2 \\ \mathrm{yb}_2 - 1 \\ \mathrm{ya}_4 - 1 \\ \mathrm{ya}_5 + \gamma * (\mathrm{ya}_4 + 1) \\ \mathrm{yb}_4 \\ \mathrm{ya}_6 - 1 \\ \mathrm{yb}_6 \end{bmatrix} \tag{20}$$

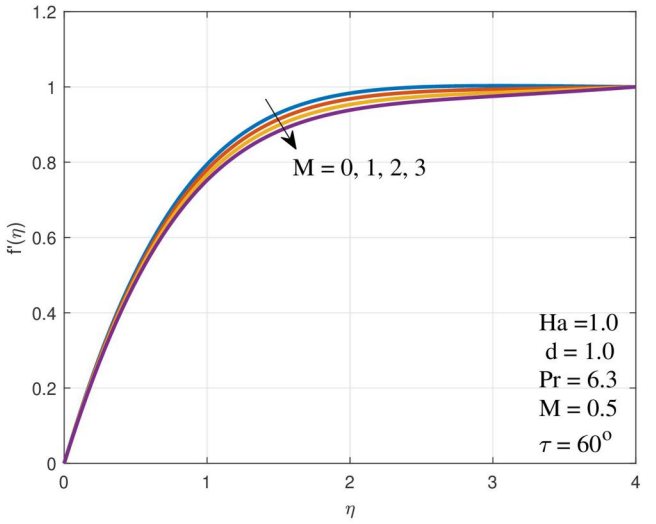

Figure 3. Plot of $f\prime(\eta)$ for different values of M.

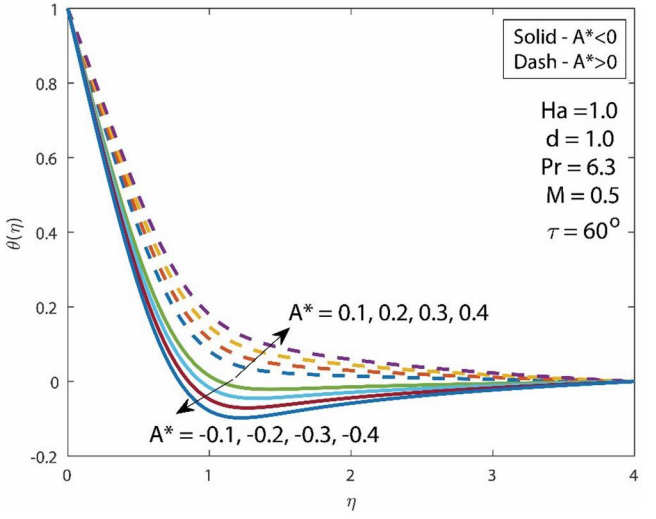

Figure 4. Variation of temperature $\theta(\eta)$ for $(A* > 0)$ and $(A* < 0)$.

3. Results and discussion

The primary motive of this section is to summarize this research. Graphs are used to depict and explain the results in detail.

The outcome of numerous parameters such as Hartmann number, MHD, internal heat generation and heat absorption, Schmidt number, Chemical reaction parameter, that determine the fluid flow and heat transfer characteristics of ternary nanofluids has been studied numerically and represented *via* graphs. Through graphs, the essential engineering aspects Cf_x, Nu_x, and Sh_x are also examined. The computational values of Skin-friction and Nusselt number with different fixed parameters are presented in Table 2 and Table 3, respectively, which found exceptional corelation with previous results.

Figures 2 and 3 display the curves of $f'(\eta)$ for distinct values of Ha and M have been determined at specific values of other parameters. We observed a reasonable rise in the curves of $f'(\eta)$

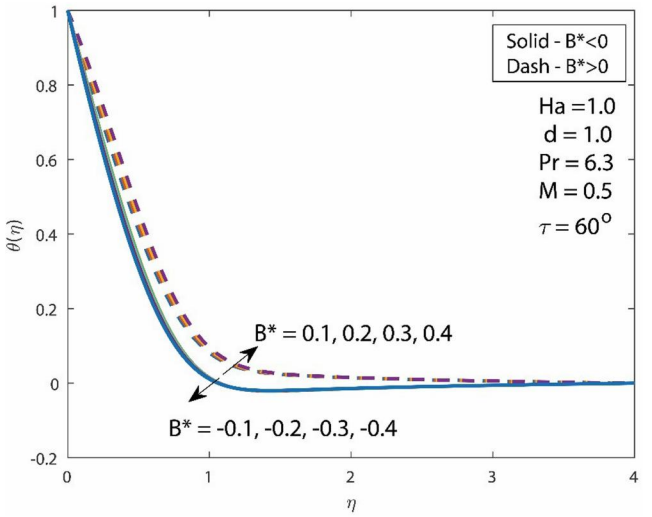

Figure 5. Variation of temperature $\theta(\eta)$ for $(B* > 0)$ and $(B* < 0)$.

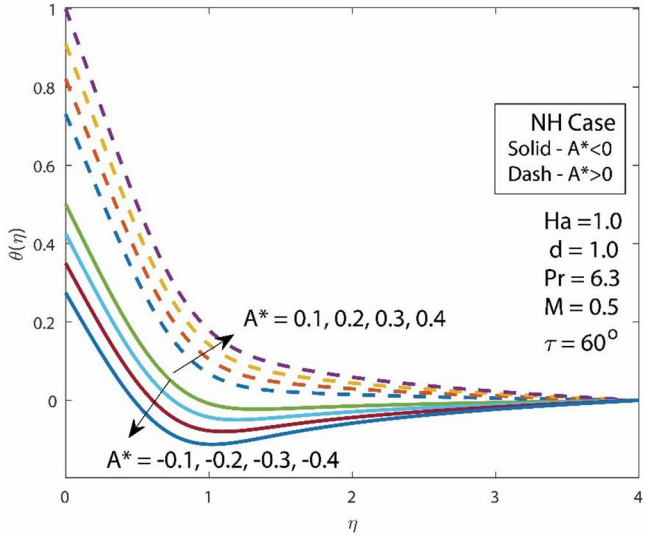

Figure 6. Effect of Newtonian heating on a $\theta(\eta)$ for $(A* > 0)$ and $(A* < 0)$.

as the value of *Ha* is increased, Physically, rise in *Ha* decreases viscous force in the fluid flow owing to increase fluid flow velocity. As *M* is varied in an increasing manner, reduction in the fluid velocity is seen in Figure 2. It is due to fact that magnetic field produces Lorentz force which hinders motion of fluid particles, resulting in drop of fluid velocity.

Figures 4 and 5 demonstrate the impact of a nonuniform heat generation and absorption on temperature distributions. The fluid's thermal distribution rises as a result of the existence of a heat generation $(A* > 0 \ and \ B* > 0)$, where the thermal boundary layer generates energy and the thermal distribution drops as a result of the heat absorption $(A* < 0 \ and \ B* < 0)$ absorbing the heat energy from the boundary layer. From physical point of view, spike in heat generation increases temperature in the fluid flow, promoting thermal distribution, whereas in the case of heat absorption, it absorbs the heat from the material leading to decrease in the temperature profile.

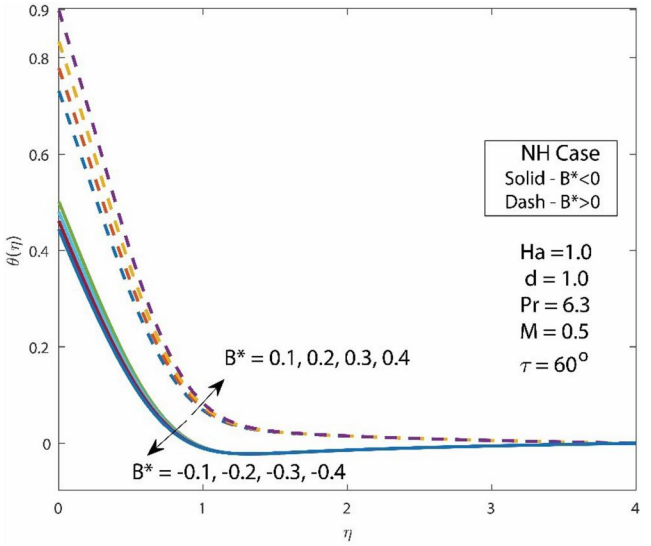

Figure 7. Effect of Newtonian heating on a $\theta(\eta)$ for $(B* > 0)$ and $(B* < 0)$.

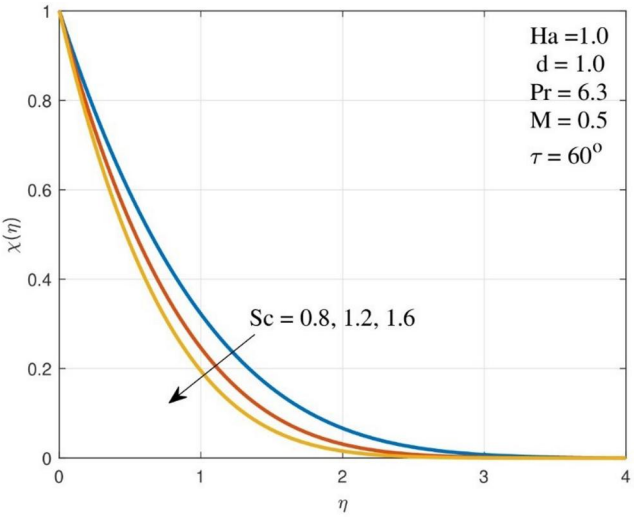

Figure 8. Nature of *Sc* over $\chi(\eta)$.

In Figures 6 and 7, due to the presence of the Newtonian heating, temperature distribution is enhanced when compared with Figures 4 and 5 where there is the absence of Newtonian heating effect. From physical standpoint, presence of Newtonian heating increases the heating of fluid due to heat generated by viscous dissipation followed by enhancing the temperature profile.

The nature of the concentration profile under the influence of the Schmidt number is described in Figure 8. It is evident from that figure the concentration profile declines as the Schmidt number rises. Owing to mass diffusivity and the Schmidt number having an inverse relationship. A fluid flow domain with a higher Schmidt number entails decreasing mass diffusion values as the concentration decreases.

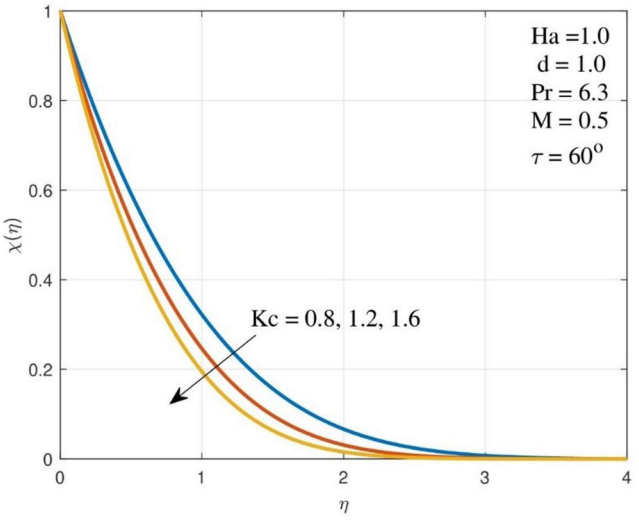

Figure 9. Nature of *Kc* over $\chi(\eta)$.

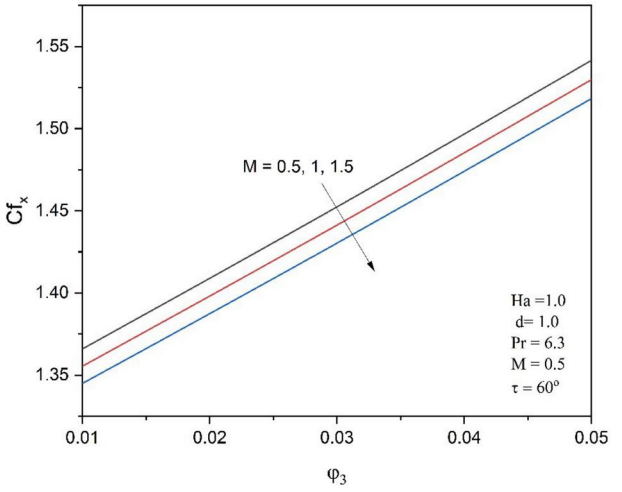

Figure 10. Plot of Cf_x on φ_3 for different values of *M*.

Figure 9 illustrates that increasing the chemical reaction constraint significantly reduces the concentration profile because is obvious that as the Kc is amplified, the solute molecules involved in the chemical reaction grow, and also as the value of Kc is increased it results in smoother access of the fluid molecules close to the boundary which diminishes the associated solute boundary layer. This result shows a great parallel outcome with that obtained by Bejawada [48].

The behavior of the skin friction coefficient against the φ_3 is depicted in Figure 10. An upsurge in *M* will reduce surface drag force (Cf_x). This is caused by a rise in φ_3, which increases the boundary layer thickness and slows down the motion of the fluid. Additionally, a rise in φ_3 displays Lorentz force in the occurrence of a MHD, which also hampers the mobility of ferro-oxide nanoparticles in the fluid. These two factors will have a prompt effect on the surface drag force. This feature contributes to reducing friction and extending the machine's life in the automotive industry.

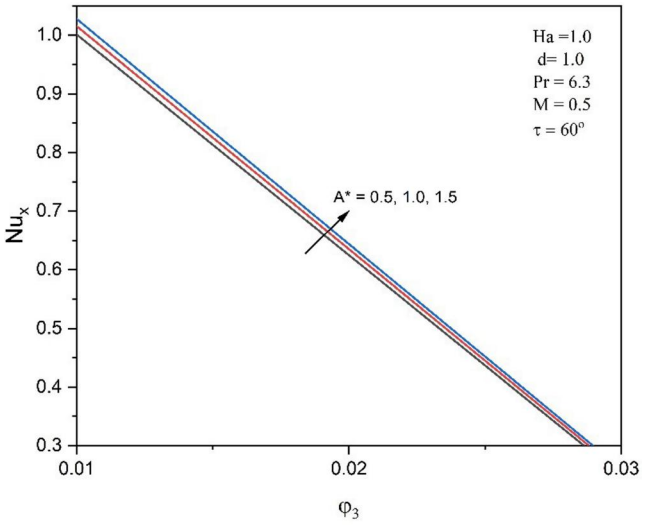

Figure 11. Plot of Nu_x over φ_3 for several values of $A* > 0$.

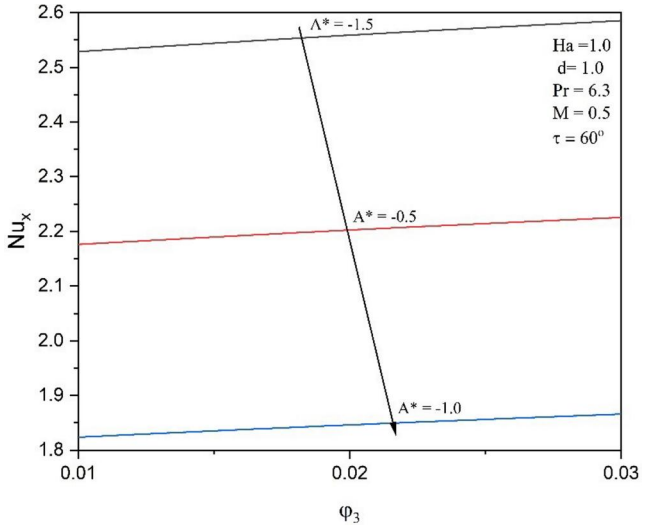

Figure 12. Plot of Nu_x over φ_3 for $A* < 0$.

Figure 11 shows the evolution of the local Nusselt number versus φ_3 the. The increase in the concentration of φ_3 enhances the heat transfer rate, so the addition of heat source $A* > 0$ which acts as a heat generator aids the heat transfer process at the boundary thermal layer whereas in Figure 12 the $A* < 0$ where the absorption of heat energy takes place lowers the heat transfer rate at the boundary. Figure 13 illustrates the relationship between the Sherwood number and volume fraction. Therefore, a rise in chemical reaction increases atom/molecule interaction, which leads to a upsurge in mass transfer rate, and hence the Sherwood number consequently rises. φ_3. Chemical reactions occur as a result of the bombarding of atoms, molecules, and ions, and they make up the fundamental basis for all chemical processes in nature and industry.

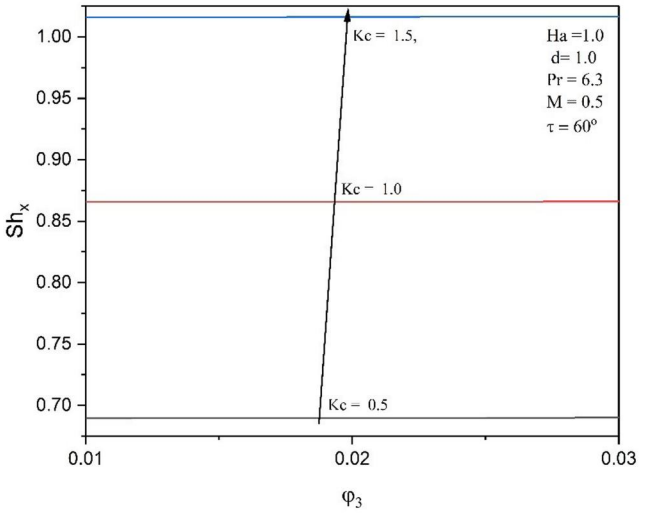

Figure 13. Plot of sh_x on φ_3 for Kc.

4. Conclusion

A theoretical model of a ternary nanofluid of MHD fluid flow was instigated to analyze the heat transfer in presence of Newtonian heating over a Riga plate with nonuniform heat generation/absorption, chemical reaction. The governing equations are developed using proper assumptions with suitable similarity variables to convert a bunch of PDEs into ODEs. Later on, these reduced equations were studied numerically using the bvp4c package. The graphs for many constraints and key engineering factors are thoroughly addressed. In the previous study [33], author examined nanofluid flow over a vertical Riga plate subjected to convective boundary conditions. TNF is taken into account for better heat transmission, also extended the study with inclined magnetic field, nonlinear heat absorption/generation, and chemical reaction subjected to Newtonian heating.

The main conclusions from the aforementioned observation are outlined below.

1. The velocity profile rises when the Hartmann number increased and falls when the magnetic parameter goes up.
2. The influence of Newtonian heating across walls can be seen in the temperature profile as a significant improvement in heat transfer and temperature distribution.
3. When the Sc and Kc is altered, the concentration profile exhibits similar characteristics.
4. Varying in M and φ_3 drop the Cf_x.
5. Heat transfer rate increases for heat generation and decreases for heat absorption.
6. Under the influence of chemical reaction there is a rise in Sherwood number for increasing values of φ_3.

This study is limited to different nanofluids and can be extended by considering different effects with different fluids such as hybrid nanofluids, CNTs and more over other geometries with different physical conditions.

Disclosure statement

No potential conflict of interest was reported by the author(s).

Funding

LMP acknowledges financial support from ANID through Convocatoria Nacional Subvención a Instalación en la Academia Convocatoria Año 2021, Grant SA77210040.

ORCID

H. F. Oztop http://orcid.org/0000-0002-2161-0639

References

[1] A. Can, F. Selimefendigil, and H. F. Öztop, "A review on soft computing and nanofluid applications for battery thermal management," *J. Energy Storage*, vol. 53, pp. 105214, Sep. 2022. DOI: 10.1016/j.est.2022.105214.

[2] S. U. S. Choi and J. Eastman, "Enhancing thermal conductivity of fluids with nanoparticles," *Proc. ASME IMECE*, Jan. 1995.

[3] S. Manjunatha, V. Puneeth, B. J. Gireesha, and A. J. Chamkha, "Theoretical study of convective heat transfer in ternary nanofluid flowing past a stretching sheet," *J. Appl. Comput. Mech.*, vol. 8, no. 4, pp. 1279–1286, Oct. 2022. DOI: 10.22055/jacm.2021.37698.3067.

[4] H. Adun, D. Kavaz, and M. Dagbasi, "Review of ternary hybrid nanofluid: synthesis, stability, thermophysical properties, heat transfer applications, and environmental effects," *J. Clean. Prod.*, vol. 328, pp. 129525, Dec. 2021. DOI: 10.1016/j.jclepro.2021.129525.

[5] X. Yang, A. Boroomandpour, S. Wen, D. Toghraie, and F. Soltani, "Applying artificial neural networks (ANNs) for prediction of the thermal characteristics of water/ethylene glycol-based mono, binary and ternary nanofluids containing MWCNTs, titania, and zinc oxide," *Powder Technol.*, vol. 388, pp. 418–424, Aug. 2021. DOI: 10.1016/j.powtec.2021.04.093.

[6] M. I. Kopp, V. V. Yanovsky, T. Anusha, and U. S. Mahabaleshwar, "MHD flow and heat transfer of a ternary hybrid ferrofluid over a stretching/shrinking porous sheet with the effects of Brownian diffusion and thermophoresis," *East Eur. J. Phys.*, vol. 1, no. 1, pp. 7–18, Mar. 2023. DOI: 10.26565/2312-4334-2023-1-01.

[7] J.-E. Cha, Y.-C. Ahn, and M.-H. Kim, "Flow measurement with an electromagnetic flowmeter in two-phase bubbly and slug flow regimes," *Flow Meas. Instrum.*, vol. 12, no. 5–6, pp. 329–339, Jan. 2002. DOI: 10.1016/S0955-5986(02)00007-9.

[8] S. Rashidi, J. A. Esfahani, and M. Maskaniyan, "Applications of magnetohydrodynamics in biological systems-a review on the numerical studies," *J. Magn. Magn. Mater.*, vol. 439, pp. 358–372, 2017. DOI: 10.1016/j.jmmm.2017.05.014.

[9] G. Mandal and D. Pal, "Estimation of entropy generation and heat transfer of magnetohydrodynamic quadratic radiative Darcy–Forchheimer cross hybrid nanofluid (GO + Ag/kerosene oil) over a stretching sheet," *Numer. Heat TR A-Appl.*, vol. 84, pp. 1–24, Apr. 2023. DOI: 10.1080/10407782.2022.2163944.

[10] G. Mandal and D. Pal, "Stability analysis of radiative-magnetic hybrid nanofluid slip flow due to an exponentially stretching/shrinking permeable sheet with heat generation," *Int. J. Ambient Energy*, vol. 44, no. 1, pp. 1349–1360, Dec. 2023. DOI: 10.1080/01430750.2023.2173651.

[11] D. Pal and G. Mandal, "Stability analysis and implication of Darcy magnetic-radiative hybrid reactive nanofluid heat transfer over a shrinkable surface with Ohmic heating," *J. Therm. Anal. Calorim.*, vol. 148, no. 5, pp. 2087–2104, Jan. 2023. DOI: 10.1007/s10973-022-11797-4.

[12] D. Pal, G. Mandal, K. Vajravelu, and W. Al-Kouz, "MHD thermo-radiative heat transfer characteristics of carbon nanotubes based nanofluid over a convective expanding sheet in a porous medium with variable thermal conductivity," *Int. J. Model. Simul.*, pp. 1–12, Jul. 2023. DOI: 10.1080/02286203.2023.2237847.

[13] G. P. Ashwinkumar, "Computational analysis on MHD Sakiadis flow of hybrid nanoliquid past an incessantly moving thin needle," *Int. J. Model. Simul.*, vol. 0, no. 0, pp. 1–12, May 2023. DOI: 10.1080/02286203.2023.2212345.

[14] S. Nadeem and S. Akram, "Influence of inclined magnetic field on peristaltic flow of a Williamson fluid model in an inclined symmetric or asymmetric channel," *Math. Comput. Model*, vol. 52, no. 1–2, pp. 107–119, Jul. 2010. DOI: 10.1016/j.mcm.2010.02.001.

[15] K.-E. Aslani, U. S. Mahabaleshwar, J. Singh, and I. E. Sarris, "Combined effect of radiation and inclined MHD flow of a micropolar fluid over a porous stretching/shrinking sheet with mass transpiration," *Int. J. Appl. Comput. Math.*, vol. 7, no. 3, pp. 60, Apr. 2021. DOI: 10.1007/s40819-021-00987-7.

[16] U. S. Mahabaleshwar, K. N. Sneha, A. Miyara, and M. Hatami, "Radiation effect on inclined MHD flow past a super-linear stretching/shrinking sheet including CNTs," *Waves Random Complex Media*, vol. 0, no. 0, pp. 1–22, Mar. 2022. DOI: 10.1080/17455030.2022.2053238.

[17] F. Selimefendigil and H. F. Öztop, "Combined effects of using multiple porous cylinders and inclined magnetic field on the performance of hybrid nanoliquid forced convection," *J. Magn. Magn. Mater.*, vol. 565, pp. 170137, Jan. 2023. DOI: 10.1016/j.jmmm.2022.170137.

[18] N. K. Manna, N. Biswas, D. K. Mandal, U. K. Sarkar, H. F. Öztop, and N. Abu-Hamdeh, "Impacts of heater-cooler position and Lorentz force on heat transfer and entropy generation of hybrid nanofluid convection in quarter-circular cavity," *HFF*, vol. 33, no. 3, pp. 1249–1286, Jan. 2022. DOI: 10.1108/HFF-07-2022-0402.

[19] K. Hiemenz, "Die Grenzschicht an einem in den gleichförmigen Flüssigkeitsstrom eingetauchten geraden Kreiszylinder." [Online]. Available: https://www.semanticscholar.org/paper/Die-Grenzschicht-an-einem-in-den-gleichf%C3%B6rmigen-Hiemenz/d864aec54cab42216097b9b4d8f7519d377b616e. Accessed: Apr. 21, 2023.

[20] F. Homann, "Der Einfluss grosset Zahigkeit bei der Stromung um den Zylinder and um die Kugel," *Z Angew Math. Mech.*, vol. 16, no. 3, pp. 153–164, 1936. DOI: 10.1002/zamm.19360160304.

[21] L. Howarth, "The boundary layer equations in three-dimensional flow," *Part II. The Flow near a Stagnation-Point. Philos. Mag.*, vol. 42, no. 335, pp. 1433–1440, 1951. DOI: 10.1080/14786445108560962.

[22] A. Ishak, K. Jafar, R. Nazar, and I. Pop, "MHD stagnation point flow towards a stretching sheet," *Phys. A: Stat. Mech. Appl.*, vol. 388, no. 17, pp. 3377–3383, Sep. 2009. DOI: 10.1016/j.physa.2009.05.026.

[23] T. Anusha, H.-N. Huang, and U. S. Mahabaleshwar, "Two dimensional unsteady stagnation point flow of Casson hybrid nanofluid over a permeable flat surface and heat transfer analysis with radiation," *J. Taiwan Inst. Chem. Eng.*, vol. 127, pp. 79–91, Oct. 2021. DOI: 10.1016/j.jtice.2021.08.014.

[24] G. P. Ashwinkumar, "Chapter 5 – Mathematical model for incompressible unsteady nanofluid fluid flow with heat and mass transfer application: comparative study on significance of space and time dependent internal heat source/sink on unsteady flow of methanol-based nanofluid over elongated sheet with or without magnetic field effect," in *Micro and Nanofluid Convection with Magnetic Field Effects for Heat and Mass Transfer Applications Using MATLABC*, S. K. Raju, I. Khan, S. S. K. Raju, and M. S. Upadhya, Eds. Elsevier, 2022, pp. 75–90. DOI: 10.1016/B978-0-12-823140-1.00004-X.

[25] A. G. Poojari, R. B, S. N, and C. Sulochana, "Enhanced heat transmission in unsteady magneto-nanoliquid flow due to a nonlinear extending sheet with convective boundary conditions," *Numer. Heat Tr A-Appl.*, vol. 0, no. 0, pp. 1–22, May 2023. DOI: 10.1080/10407782.2023.2207730.

[26] N. Sandeep, R. S. Babu, P. Nanda, and G. P. Ashwinkumar, "Enhanced heat transmission in conical slip flow of Walter's-B nanofluid," *Int. J. Mod. Phys. B*, pp. 2450096, Apr. 2023. DOI: 10.1142/S0217979224500966.

[27] P. Nanda, N. Sandeep, C. Sulochana, and G. P. Ashwinkumar, "Enhanced heat transmission in methanol-based AA7072/AA7075 tangent hyperbolic hybrid nanofluid flow along a nonlinear expandable surface," *Numer. Heat Tr A-Appl.*, vol. 83, no. 7, pp. 711–725, Apr. 2023. DOI: 10.1080/10407782.2022.2157916.

[28] N. Sandeep, P. Nanda, and G. P. Ashwinkumar, "Transpiration effect on Falkner-Skan bioconvective mixed nanoliquid flow above a poignant wedge," *Proc. Inst. Mech. Eng., Part C*, vol. 237, no. 8, pp. 1793–1805, Apr. 2023. DOI: 10.1177/09544062221134387.

[29] M. S. Abel and M. M. Nandeppanavar, "Heat transfer in MHD viscoelastic boundary layer flow over a stretching sheet with non-uniform heat source/sink," *Commun. Nonlinear Sci. Numer. Simul.*, vol. 14, no. 5, pp. 2120–2131, May 2009. DOI: 10.1016/j.cnsns.2008.06.004.

[30] K. Vajravelu and A. Hadjinicolaou, "Heat transfer in a viscous fluid over a stretching sheet with viscous dissipation and internal heat generation," *Int. Commun. Heat Mass Transf.*, vol. 20, no. 3, pp. 417–430, May 1993. DOI: 10.1016/0735-1933(93)90026-R.

[31] D. Pal and G. Mandal, "Thermal radiation and MHD effects on boundary layer flow of micropolar nanofluid past a stretching sheet with non-uniform heat source/sink," *Int. J. Mech. Sci.*, vol. 126, pp. 308–318, Jun. 2017. DOI: 10.1016/j.ijmecsci.2016.12.023.

[32] V. P. Motulevich, "Impact of chemical reactions upon heat transfer," *J. Hazard. Mater.*, vol. 46, no. 2–3, pp. 225–229, Apr. 1996. DOI: 10.1016/0304-3894(95)00074-7.

[33] U. S. Mahabaleshwar, K. R. Nagaraju, P. N. Vinay Kumar, and M. N. Azese, "Effect of radiation on thermosolutal Marangoni convection in a porous medium with chemical reaction and heat source/sink," *Phys. Fluids*, vol. 32, no. 11, pp. 113602, Nov. 2020. DOI: 10.1063/5.0023084.

[34] P. Mallikarjun, R. Murthy, U. Mahabaleshwar, and G. Lorenzini, "Numerical study of mixed convective flow of a couple stress fluid in a vertical channel with first order chemical reaction and heat generation/absorption," *MMEP*, vol. 6, no. 2, pp. 175–182, Jun. 2019. DOI: 10.18280/mmep.060204.

[35] N. Sandeep, C. Sulochana, and G. Ashwinkumar, "Understanding the dynamics of chemically reactive Casson liquid flow above a convectively heated curved expanse," *Proc. Inst. Mech. Eng., Part C*, vol. 236, no. 24, pp. 11420–11430, Dec. 2022. DOI: 10.1177/09544062221115084.

[36] J. H. Merkin, "Natural-convection boundary-layer flow on a vertical surface with Newtonian heating," *Int. J. Heat Fluid Flow*, vol. 15, no. 5, pp. 392–398, Oct. 1994. DOI: 10.1016/0142-727X(94)90053-1.

[37] T. Hayat, S. Farooq, B. Ahmad, and A. Alsaedi, "Homogeneous-heterogeneous reactions and heat source/sink effects in MHD peristaltic flow of micropolar fluid with Newtonian heating in a curved channel," *J. Mol. Liq.*, vol. 223, pp. 469–488, Nov. 2016. DOI: 10.1016/j.molliq.2016.08.067.

[38] G. Kotha, V. S. R. Munagala, V. K. Damerla, and R. S. R. Gorla, "Newtonian heating effect on laminar flow of Casson fluids: thermal analysis," *Heat Trans.*, vol. 49, no. 4, pp. 2390–2405, 2020. DOI: 10.1002/htj.21727.

[39] A. Gailitis and O. Lielausis, "On a possibility to reduce the hydrodynamic resistance of a plate in aelectrolyte," *Appl. Magnetohydrodynam.*, vol. 12, pp. 143–146, 1961.

[40] E. Magyari and A. Pantokratoras, "Aiding and opposing mixed convection flows over the riga-plate," *Commun. Nonlinear Sci. Numer. Simul.*, vol. 16, no. 8, pp. 3158–3167, Aug. 2011. DOI: 10.1016/j.cnsns.2010.12.003.

[41] H. Upreti, A. K. Pandey, Z. Uddin, and M. Kumar, "Thermophoresis and Brownian motion effects on 3D flow of Casson nanofluid consisting microorganisms over a Riga plate using PSO: a numerical study," *Chin. J. Phys.*, vol. 78, pp. 234–270, Aug. 2022. DOI: 10.1016/j.cjph.2022.06.019.

[42] N. S. Khashi'ie, I. Waini, N. S. Wahid, N. M. Arifin, and I. Pop, "Unsteady separated stagnation point flow due to an EMHD riga plate with heat generation in hybrid nanofluid," *Chin. J. Phys.*, vol. 81, pp. 181–192, Feb. 2023. DOI: 10.1016/j.cjph.2022.10.010.

[43] R. Ahmad, M. Mustafa, and M. Turkyilmazoglu, "Buoyancy effects on nanofluid flow past a convectively heated vertical riga-plate: a numerical study," *Int. J. Heat Mass Transf.*, vol. 111, pp. 827–835, Aug. 2017. DOI: 10.1016/j.ijheatmasstransfer.2017.04.046.

[44] N. M. Sarif, M. Z. Salleh, and R. Nazar, "Numerical solution of flow and heat transfer over a stretching sheet with newtonian heating using the Keller box method," *Procedia Eng.*, vol. 53, pp. 542–554, Jan. 2013. DOI: 10.1016/j.proeng.2013.02.070.

[45] J. R. Konda, M. R. N.p, R. Konijeti, and A. Dasore, "Effect of non-uniform heat source/sink on MHD boundary layer flow and melting heat transfer of Williamson nanofluid in porous medium," *MMMS*, vol. 15, no. 2, pp. 452–472, Jan. 2018. DOI: 10.1108/MMMS-01-2018-0011.

[46] R. P. Sharma, J. K. Madhukesh, S. Shukla, and B. C. Prasannakumara, "Numerical and Levenberg–Marquardt backpropagation neural networks computation of ternary nanofluid flow across parallel plates with Nield boundary conditions," *Eur. Phys. J. Plus*, vol. 138, no. 1, pp. 63, Jan. 2023. DOI: 10.1140/epjp/s13360-023-03680-4.

[47] G. K. Ramesh and B. J. Gireesha, "Non-linear radiative flow of nanofluid past a moving/stationary riga plate," *Front. Heat Mass Transf.*, vol. 9, Aug. 2017. DOI: 10.5098/hmt.9.3.

[48] H. F. Oztop and E. Abu-Nada, "Numerical study of natural convection in partially heated rectangular enclosures filled with nanofluids," *Int. J. Heat Fluid Flow*, vol. 29, no. 5, pp. 1326–1336, 2008. DOI: 10.1016/j.ijheatfluidflow.2008.04.009.